Journal of Food Health and Bioenvironmental Science
Journal homepage : http://jfhb.dusit.ac.th/

Potential Applications of Colloidal Bacterial Cellulose Nanocrystal Suspensions for Mitigating Hazardous $PM_{2.5}$ Pollution

Benyapha Kheawmanee, Arisara Thawornporn, & Tewarak Parnklang*

Faculty of Applied Science, King Mongkut's University of Technology North Bangkok, Bangkok, 10800 Thailand

Article info

Article history:
Received : 26 April 2024
Revised : 17 July 2024
Accepted : 29 July 2024

Keywords:
Bacterial cellulose, Cellulose nanocrystals, $PM_{2.5}$, Air pollution

Abstract

$PM_{2.5}$ has brought about unprecedented challenges to the atmospheric environment, air quality, and human health. Practical strategies for controlling the $PM_{2.5}$ pollution at the community level are crucial. In this research, colloidal cellulose nanocrystal suspensions are developed as a sprayable $PM_{2.5}$ remover. Bacterial cellulose nanocrystals (BCNCs) are extracted from nata de coco by sulfuric acid hydrolysis. Fourier transform infrared (FT-IR) spectroscopy reveals that the extracted product possesses β-glycosidic linkage, C-O, C-H, and O-H stretching vibrations that are similar to those of starting bacterial cellulose pellicles. Transmission electron microscopy has revealed that BCNC particles possess a rod-like morphology. These particles are characterized by an average length of approximately 800 nm and an average diameter of about 53 nm. This observation underscores the detailed structural features of BCNC particles, which are critical for understanding their properties and potential applications. The average hydrodynamic diameter assessed using dynamic light scattering has been established within the range of 300–400 nm. The crystallinity of the BCNC particle is 69% as investigated by X-ray diffraction. The negative zeta potentials attributed to the sulfate half-ester groups of BCNCs are in the range from −50 to −55 mV. The colloidal BCNC suspensions are tested for their $PM_{2.5}$ capture ability by an in-house apparatus and compared with the $PM_{2.5}$ capture efficiency of water microdroplets. It was found that the colloidal BCNC suspensions are effective for removing $PM_{2.5}$ with the $PM_{2.5}$ removal efficiency of 77.8%. The $PM_{2.5}$ removal efficiency of the colloidal BCNC suspensions is enhanced for at least 58% when compared to that of water microdroplets. The mechanism for $PM_{2.5}$ capture by the colloidal BCNC suspensions is also proposed.

Introduction

Particulate matter (PM) pollution comprising suspended particles is increasingly recognized as a pervasive issue affecting the global community. This form of pollution presents both immediate and enduring challenges to human health, disrupts the nutrient balance of natural water bodies, and influences climate patterns

* Corresponding Author
e-mail: tewarak.p@sci.kmutnb.ac.th

(Fantke et al., 2019). PM is typically categorized into two main groups based on their aerodynamic diameters: $PM_{2.5}$ and PM_{10}, which have aerodynamic diameters smaller than 2.5 μm and 10 μm, respectively (Gao et al., 2017). The harmful effects of PM pollutants are mainly discriminated by their diameters. While PM_{10} or larger PM particles could be filtered and intercepted by respiratory organs (Kuo et al., 2014), $PM_{2.5}$ pollution is particularly harmful. $PM_{2.5}$ particles have the ability to infiltrate the bronchial passages and further migrate into extrapulmonary organs and the central nervous system via the circulatory system (Zhang et al., 2019). Extended exposure to $PM_{2.5}$ may lead to a variety of health issues including airway inflammation, impaired lung function (Xing et al., 2016), $PM_{2.5}$-associated premature mortality from endpoints such as cardiovascular disease and lung cancer (Apte et al., 2015), hypertension (Pui et al., 2014), induction/exacerbation of diabetes mellitus (Feng et al., 2016), and increasing morbidity and mortality (Song et al., 2017).

Commonly employed dry techniques for mitigating indoor $PM_{2.5}$ concentrations include the use of portable air cleaners and air-conditioning systems that are equipped with porous filters. Portable air cleaners are capable of reducing particulate matter concentrations by approximately 32% to 68% (Cai et al., 2019). Over time, filters and adsorbents that have been in prolonged use demonstrate diminished efficacy attributable to saturation, increased differential pressure, and the unavoidable necessity for regeneration or replacement (Mata et al., 2022). For industrial scale, water droplets and water-spraying system are commonly employed for capture airborne dust (Bałaga et al., 2021). The efficacy of dust removal hinges upon both the mean diameter of water droplets (Kim et al., 2020) and the surface characteristics of dust particles (Carotenuto et al., 2010). PM_{10} can be effectively reduced by spraying water, achieving efficiencies as high as 98% (Wang et al., 2019; Wang et al., 2015; Wang et al., 2022). Microscale water droplets could be employed for removing PM particles. Water microdroplets generated by ultrasonic atomization with average diameters of 2, 3, and 5 μm could eliminate indoor $PM_{2.5}$ with the removal efficiencies of 56.2%, 39.2, and 34.2%, respectively (Kim & Lee, 2020). Additional modifications to the water microdroplet properties are required to improve the $PM_{2.5}$ capture efficiency so that the threshold value of 56% could be surpassed. Additionally, the efficiency of water in removing $PM_{2.5}$ still has significant potential for improvement, necessitating the incorporation of additional capture agents.

Water spray augmented with surfactants represents a highly effective method for dust suppression. This technology consistently demonstrates a direct dust suppression efficiency ranging between 80 and 95% (Li et al., 2021). Theoretically, the application of surfactants may enhance the wettability of hydrophobic dust surfaces, particularly in the case of coal dust. Consequently, this improvement in wettability can lead to a significant increase in the efficiency of dust suppression (Chang et al., 2021). Anionic surfactants (Xu et al., 2019), and non-ionic surfactants (P. Wang et al., 2020; Yuan et al., 2020) are commonly utilized for increasing dust suppression efficiency. The dust suppression efficacy of water spray incorporated with anionic surfactants typically surpasses that of water spray unaided. Surfactant-based dust suppressors, such as hydroxypropyl guar gum (Zhang et al., 2020) and sodium carboxymethylcellulose (Borowski et al., 2022) were demonstrated for PM_{10} capture efficiencies ranging from 65.52% to 84.08% and 99.1%, respectively.

Recently, methylcellulose-based polymers were demonstrated as an environmentally friendly dust binder that could be employed for direct soil and mineral dust suppression and passive dust capture through filtration (Lee et al., 2020). The dust reduction efficiency and the filtration efficiency were reported to be more than 95% and more than 99%, respectively. Both PM_{10} and $PM_{2.5}$ were effectively scavenged by the methylcellulose-based polymers. Cellulose extracted from maize straw could be grafted with poly(vinyl alcohol) and employed as a renewable dust suppressant with excellent functionality and film-forming capability (H. Wang et al., 2020). Cellulose nanocrystals (CNCs) could be effectively employed for the passive suppression of particulate materials including $PM_{2.5}$ and PM_{10} as demonstrated in the air filter fabricated from CNC-coated cotton mesh fabric with the $PM_{2.5}$ capture efficiency of 94% (Udomsri et al., 2023) and electrospun poly(vinyl alcohol)/CNCs composite with the $PM_{2.5}$ capture efficiency of 99% (Zhang et al., 2019). In addition, high efficiency renewable air filter fabricated from electrospun protein nanofiber-coated cellulose microfiber fabrics (Souzandeh et al., 2017), cellulose nanofibers (CNFs) (Hung et al., 2021), CNFs/zein nanoparticles and wood pulp (Fan et al., 2019), and bacterial cellulose (Wu et al., 2022) were previously demonstrated. These prior studies suggest the possibility of utilizing cellulose-based

nanomaterials as sustainable additives to improve PM capture efficiency when combined with water spray techniques.

As cellulosic nanomaterials demonstrate significant potential in effectively capturing hazardous PM, cellulose nanocrystals extracted from bacterial cellulose (BC) pellicles, i.e. bacterial cellulose nanocrystals (BCNCs) are proposed for utilizing as dust binder additives and enhancing the $PM_{2.5}$ capture efficiency of water spray techniques. Cellulose nanocrystals has shown no pulmonary, oral, or skin cytotoxicity (Roman, 2015) and could be spontaneously eliminated from lung cell surface (Endes et al., 2015). A colloidal BCNC suspension is aerosolized into water microdroplets using a jet nebulizer and then exposed to generated $PM_{2.5}$ particles in a parallelepiped test chamber. BCNCs can impart negative charges to the water microdroplets, enhancing their interactions with the polar functional groups on the surfaces of $PM_{2.5}$ particles (Liu et al., 2015). Under optimized conditions, the aerosolized colloidal BCNC suspension improves the $PM_{2.5}$ removal efficiency for at least 58% when compared to the pure water microdroplets. Based on our observations, suspensions of 1.5% (w/v) cellulose nanocrystals, at a volume of 1.5 mL, can effectively reduce $PM_{2.5}$ concentrations from an initial concentration of ≈300 μg/m^3 in a 120-L air volume with an efficiency of up to 80%. This translates to a material cost of only 0.135 THB per treatment. Therefore, cellulose nanocrystals have significant potential as a cost-effectiveness, scalability, and safe $PM_{2.5}$ removal agent for large areas. Furthermore, the mechanism of $PM_{2.5}$ capture by the aerosolized colloidal BCNC suspension is also proposed.

Materials and methods

1. Materials

Bacterial cellulose (nata de coco) (BC) was purchased from a local manufacturer (Nakhonpathom, Thailand). Sulfuric acid (98%, AR Grade) was obtained from Merck (Darmstadt, Germany). All chemicals were used as received without further purification. Water of ultrahigh purity, specifically at 18.2 MΩ·cm, was obtained using a Sartorius arium® pro water system (Sartorius Lab Instruments GmbH & Co. KG, Goettingen, Germany). Dialysis tubing (Innovating Science®, IS13029, 32 mm × 20.4 mm, MWCO = 12–14 kDa) fabricated from regenerated cellulose derived from cotton linters was acquired from Aldon Corporation (New York, United States). The air zero characterized by an oxygen concentration of approximately 21±1%, a total hydrocarbon content under 5 ppm, and a moisture content below 15 ppm, was sourced from Linde (Thailand) Public Company Limited (Samutprakan, Thailand).

2. BC preparation

The BC pellicle pretreatment was performed according to the reported method with some modifications (Vasconcelos et al., 2017a; Yan et al., 2017). Bacterial cellulose (BC) pellicles, commonly utilized in the production of nata de coco, undergo a specific pretreatment process. Initially, these pellicles are treated with a 0.1 M solution of sodium hydroxide (NaOH) at temperatures ranging from 70–80°C for a duration of 120 min. This step is crucial for breaking down any residual chemicals or cellular material that might be present from the nata de coco manufacturing process. Following the alkali treatment, the BC pellicles are thoroughly rinsed with de-ionized water until they reach a neutral pH, ensuring the complete removal of any remaining NaOH and contaminants. This systematic purification process is essential for achieving the desired cleanliness and quality of the BC pellicles for further applications. Subsequently, the BC pellicles were carefully segmented into diminutive cubes and disintegrated in water with a Waring® 8011ES laboratory blender (Waring® Laboratory Science, Stamford CT, United States of America) for 10 min. Their suspensions were further homogenized at 15,000 rpm for 5 min with a IKA® T25 Digital ULTRA-TURRAX® high performance disperser (IKA® Works (Thailand) Co. Ltd., Bangkok, Thailand) to obtain uniform BC aqueous suspension.

3. BCNC preparation

BCNCs were extracted through a process involving the hydrolysis of cellulose using sulfuric acid. The acid hydrolysis reaction conditions are described in Table 1. The ratio of the mass of dried BC pulp and the acid volume was 1.0 g dried BC pulp per 10 mL acid (1:10 (w/v) ratio) (Ngoensawat et al., 2021). The acid volume employed for each synthesis batch was 100 mL.

Table 1 Acid hydrolysis reaction conditions employed for BCNC preparation

Sample	[H_2SO_4] (% w/w)	Hydrolysis temperature (°C)	Reaction time (min)
S-BCNC50	50	50	120
S-BCNC60	50	60	120
S-BCNC70	50	70	120

Typically, the dried BC pulp was immersed in the specified acid solution under mechanical stirring at the

specified hydrolysis temperature. After the hydrolysis reaction reached the specified reaction time, the reaction was stopped by introducing cold water at a temperature of 0°C into the reaction mixture. The resulting BCNCs were dispersed within the highly acidic medium of the reaction. To purify the obtained product, the extracted BCNC colloid was centrifuged at 9,000 rpm for 10 min using a Hettich Universal 320 R benchtop centrifuge (Andreas Hettich GmBH & Co. KG., Tuttlingen, Germany). The supernatant was carefully removed, and ultrapure water was then introduced to the residual centrifugate. This ultracentrifugation step was conducted repeatedly to achieve a supernatant pH between 2 and 3. Subsequently, the mixture underwent dialysis until the pH of the BCNC suspension stabilized within a neutral range of 6 to 7. Furthermore, an Elmasonic P60H ultrasonic cleaner (Elma Schmidbauer GmbH., Singen, Germany) was utilized to optimize the dispersion of BCNC dispersion in ultrapure water. Ultrasonication duration ranged from 2 to 5 min. Following processing, the resultant product was stored at a temperature of 4–5°C for subsequent applications (Ngoensawat et al., 2021).

4. Instrumental characterization

The dimensions and surface charges of CNCs were characterized using dynamic light scattering and electrophoretic mobility measurements using a Zetasizer SZ-100 (Horiba scientific, Kyoto, Japan). Measurements were conducted at a fixed scattering angle of 90°. The temperature within the sample holder was maintained at 25.0 ± 0.2°C. The applied electrode voltage was set at 3.4 V.

Fourier transform infrared (FT-IR) spectroscopy was utilized to analyze the functional groups present in both the initial BC pellicles and the dried BCNC powder. The BCNC powder was prepared by evaporating purified BCNC suspensions in an air-circulated oven set at 80°C until complete moisture removal. A Nicolet iS5 FT-IR spectrophotometer (Thermo Scientific, Massachusetts, United States) equipped with a fast recovery deuterated triglycine sulfate (DTGS) detector was employed for acquiring attenuated total reflectance (ATR) FT-IR spectra. A single-bounce ATR accessory with a laminate-diamond crystal (iD5) served as the sampling probe, onto which the dried specimen was positioned on a flat diamond crystal internal reflection element (IRE) with a sampling diameter of 1.5 mm. The specimen was pressed against the flat diamond crystal using a pressure device until optimal pressure was achieved. All ATR FT-IR spectra were recorded at a resolution of 4 cm^{-1}, with each spectrum comprising 32 co-added scans.

Transmission electron microscopy (TEM) analysis involved depositing drops of an aqueous suspension containing dispersed BCNC particles onto a CF-300CU support film grid (Electron Microscopy Sciences, Pennsylvania, United States). The grid was subsequently placed in a desiccator, allowing complete solvent evaporation over a minimum period of 24 hr. The resultant dried samples were examined using a JEOL JEM-2100 analytical electron microscope (JEOL Ltd., Tokyo, Japan) operated at an accelerating voltage of 200 kV. Micrographs obtained from the TEM were utilized to directly measure the lengths and diameters of the BCNC particles using ImageJ software (Schneider et al., 2012). The study determined the mean length and diameter by analyzing a minimum of 100 BCNC particles extracted from 20–30 TEM micrographs.

The degree of crystallinity in dried BCNC powder and initial BC pellicles was assessed through X-ray diffraction analysis. X-ray diffractograms were recorded using a Bruker AXS Model D8 Discover X-ray diffractometer (Bruker AXS GmbH, Karlsruhe, Germany) operating at 40 kV and 40 mA, utilizing CuKα radiation with a wavelength (λ) of 1.54060 Å. The dried samples were continuously scanned over 2θ angles ranging from 3 to 60°, with a step size of 0.0200°. The total crystallinity was determined on the basis of the Rietveld analytical method (Jordan et al., 2019) by using DIFFRAC.EVA (Version 6.0.0.7), as described by Eq. (1):

$$\%\text{Crystallinity} = \frac{\text{Crystalline Area}}{\text{Total Area}} \times 100\% \quad (1)$$

The crystallite size denoted as D_{hkl} was determined using the Scherrer's equation, as expressed in Eq. (2) (Henrique et al., 2013).

$$D_{hkl} = \frac{K\lambda}{\beta_{\frac{1}{2}} \cos\theta} \quad (2)$$

where D_{hkl} is the crystallite dimension in the direction normal to the *hkl* family of lattice planes. K is the correction factor and taken to be 1.0 (Jordan et al., 2019). λ is the radiation wavelength in nm. θ is the diffraction angle. $\beta_{\frac{1}{2}}$ is the angular peak width in radians at the half-maximum intensity. The crystallite size was calculated from the direction perpendicular to (200) lattice plane of cellulose.

5. $PM_{2.5}$ removal evaluation

The instrumental apparatus specifically designed to

evaluate the $PM_{2.5}$ removal efficiency of colloidal BCNC suspensions is schematically shown in Fig. 1 The apparatus for evaluating the $PM_{2.5}$ removal efficiency of a colloidal BCNC suspension

After measuring the background $PM_{2.5}$ levels in an airtight test chamber with dimensions of 55 cm × 55 cm × 40 cm, incense was burned to produce particulate matter, specifically $PM_{2.5}$ particles. These particles exhibited a broad size distribution, ranging from less than 300 nm to greater than 10 µm, with the majority being smaller than 1 µm in diameter (Liu et al., 2015). Notably, particulate matter from incense smoke demonstrated a $PM_{2.5}$ composition level of 99.88% (Zhang et al., 2018). The generated $PM_{2.5}$ particles were uniformly dispersed in the airtight test chamber using installed electric fans for 120 sec. The initial relative humidity in the test chamber was in the range of 5–8%. To initiate the $PM_{2.5}$ removal evaluation, air was flowed into the nebulizer (VIXONE™ Kit Nebulizer, W0217, Westmed, USA) at a rate of 3 L/min. The colloidal BCNC suspension contained in the holding chamber was aerosolized and introduced into the test chamber. The nebulizing volume of the suspension was 2.00 mL. The nebulized liquid droplets has a mass median aerodynamic diameter (MMAD) of 3.43 µm (Abdelrahman et al., 2020). The length-mean and median aerodynamic diameters of the nebulized liquid droplets determined from optical laser scattering microscopy (Wang, 1998) were 17.2 ± 4.5 µm and 16.2 µm, respectively. The nebulizing rate was measured to be 0.207 ± 0.015 mL/min. The nebulizing time was 8–10 min. After the nebulized fluid particles entered the test chamber, they were exposed to the generated $PM_{2.5}$ particles for 180 sec. The particle mixing process was facilitated by the two electric fans. Finally, the concentration of $PM_{2.5}$ particles was measured as a function of time for another 10 min. The concentration of $PM_{2.5}$ expressed in µg/m³ were quantified by a TEMTOP® M2000C particle counter manufactured by Elitech Technology, San Jose, United States. This device offers a measurement resolution of 0.1 µg/m³ and maintains an accuracy of ±10% within the concentration range of 100–500 µg/m³. The efficiency of $PM_{2.5}$ removal denoted as %E can be calculated using an amended version of the reported equation (Lee et al., 2011):

$$\%E = \frac{\left[PM_{2.5}(I) - PM_{2.5}(B)\right] - \left[PM_{2.5}(F) - PM_{2.5}(B)\right]}{\left[PM_{2.5}(I) - PM_{2.5}(B)\right]} \times 100\% \quad (3)$$

$$= \frac{PM_{2.5}(I) - PM_{2.5}(F)}{PM_{2.5}(I) - PM_{2.5}(B)} \times 100\%$$

where $PM_{2.5}$ (I) is the concentration of the generated $PM_{2.5}$ in the airtight test chamber before passing the nebulized BCNC suspensions, $PM_{2.5}$ (F) is the concentration of $PM_{2.5}$ after exposure to the nebulized BCNC suspensions, and $PM_{2.5}$ (B) is the concentration of $PM_{2.5}$ in the initial gaseous mixture of air zero and ambient air.

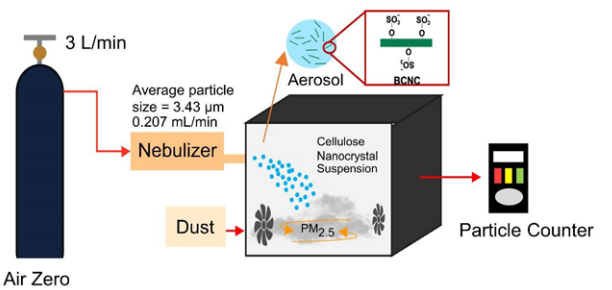

Fig. 1 The apparatus for evaluating the $PM_{2.5}$ removal efficiency of a colloidal BCNC suspension

Results and discussion

Bacterial cellulose pellicles could be employed as a source for cellulose nanocrystal extraction by mineral acid hydrolysis (Arserim-Uçar et al., 2021; Salari et al., 2019). Particularly, there are 3 main steps involved in the sulfuric acid catalyzed hydrolysis of cellulose, including the separation of microfibrils, the dissolution of amorphous cellulose region, and the sulfation of cellulose nanocrystals (Udomsri et al., 2023). Fig. 2 shows the hydrodynamic diameter distributions of BCNCs extracted from BC at the sulfuric acid hydrolysis temperature of 50, 60, and 70°C. The particle size analysis data and the colloidal stability are also summarized in Table 2.

After the hydrolysis reaction, the extracted BCNCs appeared as opaque colloidal suspension (Fig. 2A1, Fig. 2B1, and Fig. 2C1). However, the crude S-BC-NC70 sample exhibited a yellow-brown color. This indicates the excessive degradation of cellulose and the possible formation of oligosaccharide (Bouchard et al., 2016), glucose (Blanco et al., 2018), and oxidized glucose derivatives (Fachri et al., 2015). After dilution, the colloidal BCNC suspensions at all hydrolysis temperatures exhibited characteristic flow birefringence, attributable to the polyanionic character contributed by the negative charges on the cellulose nanocrystal surfaces (Habibi et al., 2006) (Fig. 2A2, Fig. 2B2, and Fig. 2C2). This evidence preliminarily supports the formation of cellulose

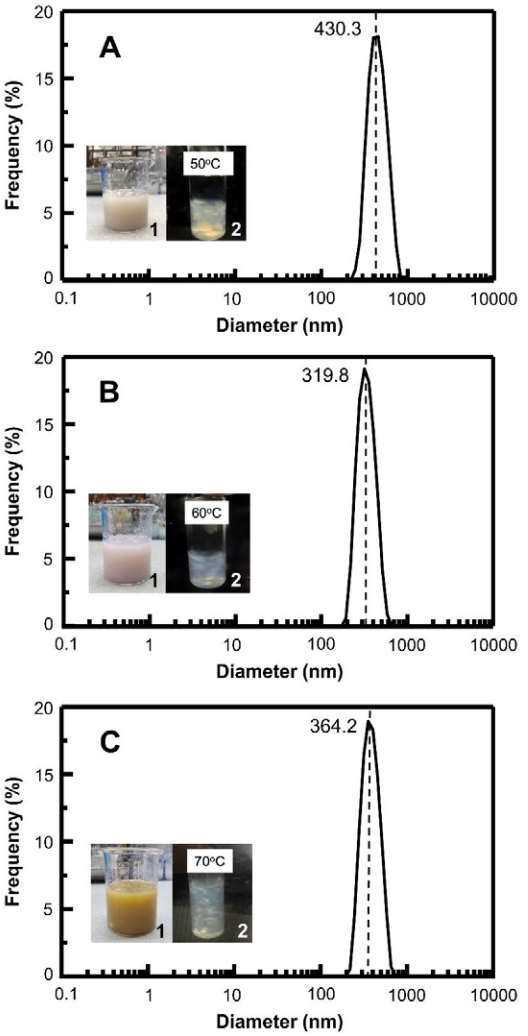

Fig. 2 Hydrodynamic diameter distributions of purified colloidal S-BCNC50 (A), S-BCNC60 (B), and S-BCNC70 (C) suspensions. The corresponding crude suspensions in beakers and their purified dilute suspensions in vials under the cross-polarized light are shown in the insets

Table 2 Particle size analysis data of BCNCs extracted by sulfuric acid hydrolysis at the temperatures of 50, 60, and 70°C

Hydrolysis Temperature (°C)	Hydrodynamic Diameter (nm)	Polydispersity Index	Zeta Potentials (mV)	Conductivity (mS/cm)
50	430.3 ± 37.1	0.275 ± 0.064	−49.7	0.238
60	319.8 ± 7.88	0.276 ± 0.004	−56.8	0.219
70	364.2 ± 18.9	0.406 ± 0.240	−52.2	0.234

nanocrystals. In addition, the extracted BCNC particles possessed negative zeta potential values at the sulfuric acid hydrolysis temperatures employed. The negative zeta potentials of the extracted BCNCs could be attributed to the sulfate half-ester groups ($-OSO_3^-$) formed by the reaction of sulfuric acid and hydroxyl groups on the surface of BCNCs during the acid hydrolysis (Delepierre et al., 2021). For the S-BCNC50 sample, the extracted BCNC particles exhibited the largest average hydrodynamic diameter of 430.3 ± 37.1 nm. Despite the higher hydrolysis temperature applied to the S-BCNC70 sample, its average hydrodynamic diameter of 364.2 ± 18.9 nm was larger than that of the S-BCNC60 sample, which measured at 319.8 ± 7.88 nm. This phenomenon aligns with observations from the sulfuric acid hydrolysis of bleached kraft pulp (Bouchard et al., 2016). The extracted cellulose nanocrystals exhibited hydrodynamic diameter of 86 ± 3 nm and 78 ± 5 nm when the hydrolysis temperatures decreased from 65 to 50°C with a constant sulfuric acid concentration of 64% (w/w). In the case of colloidal stability, the zeta potentials of purified S-BCNC70 suspension displayed the value of −52.2 mV, which was higher than that of purified S-BCNC60 suspension, i.e., −56.8 mV is in agreement with the work reported for the sulfuric acid hydrolysis of *Imperata brasiliensis grass* (Benini et al., 2018). The negative zeta potentials of –30.83 mV was obtained for cellulose nanocrystals extracted at 35°C, while the zeta potentials of −21.86 mV was observed when the hydrolysis temperature of 60°C was employed. In addition, our results also agree with the observation of Roman and Winter (2004) that BC extracted at higher sulfuric acid hydrolysis temperature was less fragmented and possessed lower surface charge densities. The process of extracting cellulose nanocrystals from pure cellulose primarily involves the use of sulfuric acid hydrolysis. This method selectively targets and breaks down the disordered or para-crystalline areas within the cellulose structure. Conversely, the crystalline regions, which are more resistant to this chemical intervention, remain unaffected. The varied rates of hydrolysis between the amorphous and crystalline domains are crucial in determining the specific sites of cleavage. The extraction of cellulose nanocrystals necessitates meticulous control of several parameters, including temperature, acid concentration, the ratio of acid to cellulose, and reaction time, to ensure consistency and reproducible results. Nevertheless, the morphology, the hydrodynamic diameters, and the zeta potential values cellulose nanocrystals are still varied according to the cellulose source employed (Habibi et al., 2010). The polydispersity index of S-BCNC70 sample possessed the value of 0.406, which was higher than that of purified S-BCNC60 colloid, i.e., 0.276. The polydispersity indices of the

purified S-BCNC60 and S-BCNC70 suspensions that were less than 0.7 imply they were "moderately monodisperse" (Mudalige et al., 2019). The conductivity values of the purified BCNC suspensions extracted at the temperature of 50–70°C displayed a comparable value in the range of 0.219–0.238 mS/cm. The conductivity value of the commercialized CelluForce® cellulose nanocrystal suspension is specified in the range that is less than 0.350 mS/cm at the solid content of 2% (w/w) in de-ionized water (Reid et al., 2017). The observed conductivity values of colloidal BCNC suspensions implied a good purification process that residual proton and sulfate ions were almost completely removed from the system.

The previous discussion suggests that the purified S-BCNC60 suspension might be optimal for further studies because the hydrolysis conditions employed were controllable and did not cause excessive cellulose degradation. In addition, the S-BCNC60 particles possess the highest negative zeta potentials of −56.8 mV. The zeta potential of S-BCNC60 particles being less than −30 mV indicates that the colloidal S-BCNC60 suspension is highly stable (Bhattacharjee, 2016). Furthermore, the good dispersion of S-BCNC60 particles might be crucial for generating uniform aerosol particles and benefit $PM_{2.5}$ capture (Fan et al., 2019). Therefore, the purified S-BCNC60 suspension was selected for further characterization.

The morphology of S-BCNC60 particles was investigated by transmission electron microscopy. The results are shown in Fig. 3. The purified S-BCNC60 cellulose nanocrystals exhibited rod-like particle shape with an average length of 876 ± 379 nm and an average diameter of 53 ± 11 nm. The particle diameter of cellulose nanocrystals is reported to be in the range of 5–70 nm (Sharma et al., 2019). For cellulose nanocrystals derived from bacterial cellulose fibers, the particle length might be in the range of 100 nm–several micrometers (Klemm et al., 2018). Similar particle morphology was also reported in the work by Roman and Winter (2004) and Arserim-Uçar et al. (2021).

FT-IR spectroscopy was employed to monitor the chemical functional groups alteration in cellulosic structure after the sulfuric acid hydrolysis. FT-IR spectra of the dried starting BC pellicles and the purified S-BCNC60 powders are shown in Error Message are shown in Fig. 4. The corresponding functional group assignments are summarized in Table 3. The FT-IR spectra of BC and S-BCNC60 display almost similar absorption pattern. A broad band in the region of 3,670-3,000 cm^{-1} indicates the O-H stretching vibration of the OH groups in cellulose molecules and intra- and intermolecular hydrogen bonding presented in cellulose and absorbed water (Kargarzadeh et al., 2012; Sheltami et al., 2012). The IR absorption peaks centered in the range of 2,892-2,894 cm^{-1} are attributed to the C-H stretching vibrations. The O-H bending vibrations of the adsorbed water molecules in cellulose structure display IR absorption peaks at 1,638 cm^{-1} and 1,643 cm^{-1} for BC and SBCNC-60 samples, respectively. The IR absorption peaks centered at 1,427-1,428 cm^{-1} are assigned to the asymmetric angular deformation of C-H bonds. The cellulose ring stretching vibrations and C-O-C asymmetric stretching at β-glycosidic linkage appeared in the FT-IR spectra of BC and S-BCNC60 at 1161 and 1,162 cm^{-1}, respectively. The IR absorption peaks at 1,030 and 1,031 cm^{-1} are ascribed to C-O at C6 stretching. The β-glycosidic linkages between the glucose units of cellulose were observed at 897 cm^{-1}. From previous discussion, most IR absorption peaks of BC and S-BCNC60 were located at approximately the same positions. These results implied that the cellulosic functional groups of BC were still preserved in S-BCNC60 after the sulfuric acid hydrolysis.

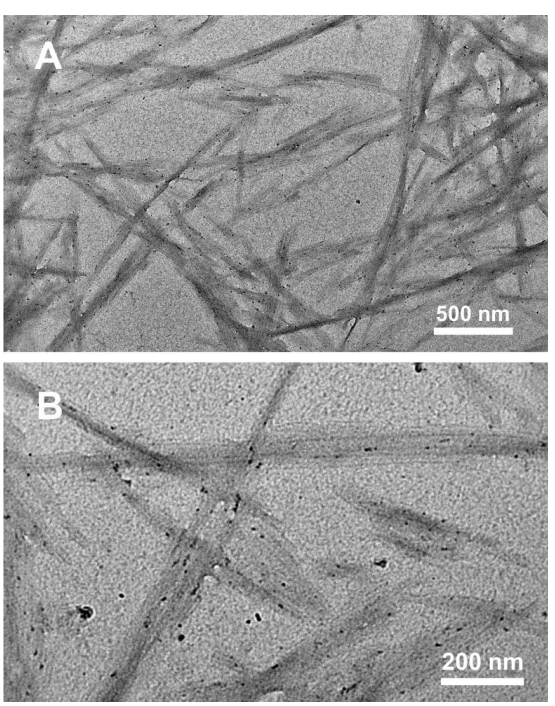

Fig. 3 TEM micrographs of the extracted S-BCNC60 cellulose nanocrystals. The scale bar in A and B are 500 nm and 200 nm, respectively

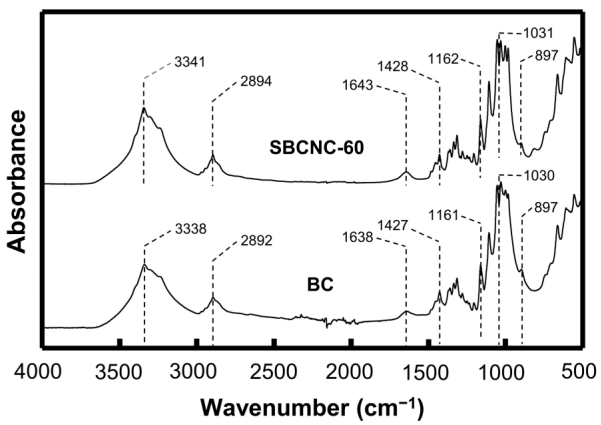

Fig. 4 FT-IR spectra of the dried bacterial cellulose (BC) and the purified BCNC powders extracted from the sulfuric acid hydrolysis at 60°C (S-BCNC60)

Table 3 Functional group assignment of the dried bacterial cellulose (BC) and the purified bacterial cellulose nanocrystal powders extracted from the sulfuric acid hydrolysis at 60°C (S-BCNC60) from their corresponding FT-IR spectra

Wavenumber (cm^{-1})		Chemical functional groups
BC	SBCNC-60	
3338	3341	O—H stretching vibrations of CH2-OH in cellulose (Jordan et al., 2019)
2892	2894	C—H stretching vibrations (Vasconcelos et al., 2017a)
1638	1643	O—H bending vibrations of the adsorbed water (Mandal & Chakrabarty, 2011)
1427	1428	asymmetric angular deformation of C—H bonds (Vasconcelos et al., 2017a)
1161	1162	C—O—C cellulose ring stretching vibrations (Braun & Dorgan, 2009) or C−O−C asymmetric stretching at β-glucosidic linkage (Han et al., 2013)
1030	1031	C—O at C6 stretching (Han et al., 2013)
897	897	β-glycosidic bonds (Mandal & Chakrabarty, 2011)

X-ray diffraction was employed to observe the crystallinity of starting BC pellicles and the extracted S-BCNC60 particles. The corresponding X-ray diffractograms are shown in Fig. 5. The XRD results are also summarized in Table 4. X-ray diffraction patterns of BC and S-BCNC60 samples displayed diffraction peaks at 2θ of 14.46° and 14.54°, 16.75° and 16.82°, and 22.53° and 22.72°, corresponding to the lattice planes (10−1), (101), and (200), respectively (Arserim-Uçar et al., 2021). In addition, these three diffraction peaks indicate the presence of cellulose type Iα (triclinic) (Henrique et al., 2015). The lattice plane (200) representing the crystalline region could be employed to determine the crystallite sizes of the BC and S-BCNC60 samples by the Scherrer's equation. The calculated crystallite sizes of BC and S-BCNC60 were 7.66 and 7.57 nm, respectively. The reduction of the crystallite sizes of BCNCs after the sulfuric acid extraction was also observed in the work by Vasconcelos et al. (2017b). The crystallinity index of S-BCNC60 increased to 69% when compared to that of the starting BC fibers, i.e., 56%. This might be due to the selective dissolution of amorphous cellulose region interconnecting the crystalline cellulose region in the starting BC fibrils by the sulfuric acid hydrolysis (Salari et al., 2019). The crystallinity index of S-BCNC60 samples is quite similar to the crystallinity index of cellulose nanocrystals extracted from cellophane by sulfuric acid hydrolysis, i.e., 68% (Henrique et al., 2015).

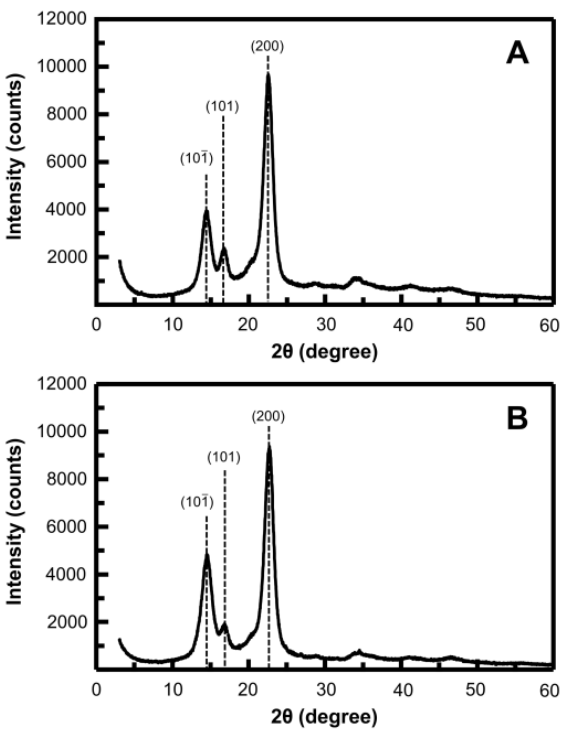

Fig. 5 X-ray diffraction patterns of the dried bacterial cellulose powder (BC) (A) and the purified bacterial cellulose nanocrystal powders extracted from the sulfuric acid hydrolysis at 60°C (S-BCNC60) (B)

Table 4 Diffraction angles and their corresponding peak intensities, the associated diffraction planes, and the crystallinity indices of the dried bacterial cellulose powder (BC) (A) and the purified bacterial cellulose nanocrystal powders extracted from the sulfuric acid hydrolysis at 60°C (S-BCNC60)

Sample	(2θ, Intensity/Counts)			Crystallinity (%)	Amorphous (%)
	(10−1)	(101)	(200)		
BC	(14.46, 3931)	(16.75, 2369)	(22.53, 9673)	56	44
SBCNC-60	(14.54, 4838)	(16.82, 1906)	(22.72, 9343)	69	31

The previous discussions confirmed the successful extraction of bacterial cellulose nanocrystals from the sulfuric acid hydrolysis of BC nanofibrils. Next, we utilized the extracted S-BCNC60 nanocrystals for $PM_{2.5}$ capture. The colloidal S-BCNC60 suspensions at the concentration determined gravimetrically of 1.62% (w/w) was aerosolized by the nebulizer kit before exposing to the model $PM_{2.5}$ pollution generated by incense burning. The results are shown in Fig. 6. The background $PM_{2.5}$ in the initial gaseous mixture in the test chamber had an average value of 16.0 ± 4.5 μg/m^3. The initial $PM_{2.5}$ concentration of the generated model pollution showed the value in the range of 150–300 μg/m^3 with the average value of 284.5 ± 32.4 μg/m^3. The concentration range is categorized as "very unhealthy" to "hazardous", according to the United States Air Quality Index (US AQI) (Mintz, 2018). When ultrapure water was employed as a $PM_{2.5}$ suppressor, its $PM_{2.5}$ removal efficiency was determined to be 19.5 ± 9.4%. Kim and Lee (2020) reported the utilization of microscale water droplet generated by the ultrasonic module of a commercial household ultrasonic humidifier for $PM_{2.5}$ elimination. Their results revealed that the water microdroplet with an average diameter of 3-5 μm could remove $PM_{2.5}$ with efficiencies in the range of 34.2-39.2% after 30 min of the atomization device operation. When the colloidal S-BCNC60 suspension was employed for the $PM_{2.5}$ removal test, the $PM_{2.5}$ removal efficiencies of 77.8 ± 5.5% was observed. This value is higher than the $PM_{2.5}$ removal efficiency of water microdroplets with an average diameter of 2 μm, i.e., 56.2% (Kim & Lee, 2020). These results suggested that BCNCs could enhance $PM_{2.5}$ capture efficiency. When compared to the nebulized ultrapure water droplets, the colloidal S-BCNC60 suspension exhibited the enhanced $PM_{2.5}$ capture efficiency up to 58%. The possible mechanism of $PM_{2.5}$ by colloidal bacterial cellulose nanocrystal suspensions is proposed as schematically shown in Fig. 7 (Li et al., 2020; Li et al., 2021). Initially, the water microdroplets and colloidal BCNC particles are dispersed through the polluted air and randomly collided with each other. The initial contact between particulate materials and aerosolized bacterial cellulose nanocrystal colloid is primarily driven by the inertial collision mechanism. The particle repulsion caused negatively charged surface of BCNC particles might facilitate the particle migration to the surfaces of water microdroplets. BCNC particles dispersed in the water microdroplets could enhance the physical adhesion of aerosolized water microdroplet surfaces and $PM_{2.5}$ particles through the van der Waals interaction, specifically ion-dipole interactions (Fan et al., 2019; Liu et al., 2015; Wu et al., 2022; Xiong et al., 2021). Additionally, charged water microdroplets could enhance the dust collection efficiency when compared to the uncharged water microdroplets (Carotenuto et al., 2010). As the water microdroplets endowed with negatively charged BCNC particles continuously collide with $PM_{2.5}$ particles, more $PM_{2.5}$ particles are adsorbed on water microdroplet surfaces and agglomerates are formed through the distribution mechanism. The $PM_{2.5}$-BCNC agglomerates are subsequently sunk to the ground by gravitational forces. Finally, as water evaporates, $PM_{2.5}$ particles remained adsorbed on BCNC particles. This prevents re-entrainment of $PM_{2.5}$ particles back to the purified air (Zhou et al., 2020).

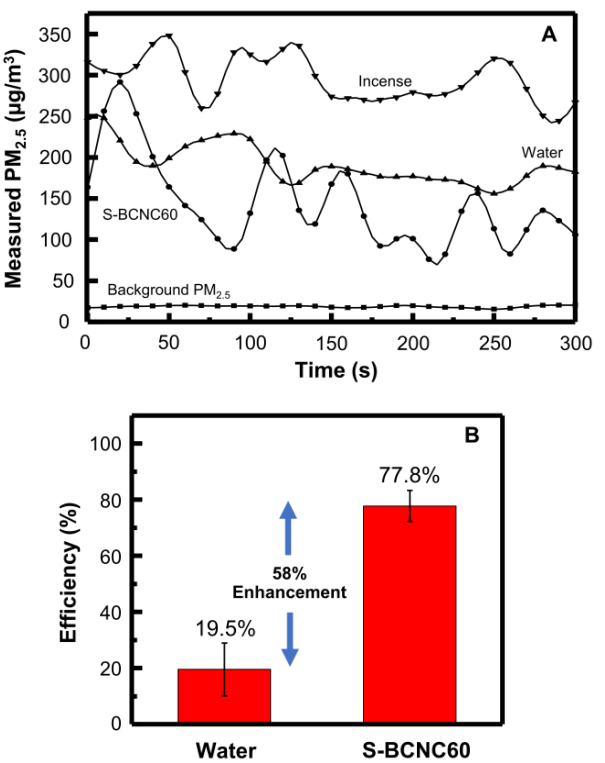

Fig. 6 Time-dependent $PM_{2.5}$ concentrations of the initial air mixture (Background $PM_{2.5}$), the model $PM_{2.5}$ pollution (incense), the gaseous mixture after passing with the nebulized de-ionized water (DW), and the gaseous mixture after exposing with the colloidal S-BCNC60 suspensions (BCNC) (A). $PM_{2.5}$ removal efficiency of the aerosolized de-ionized water (DW) and colloidal bacterial cellulose nanocrystals (S-BCNC60) are compared in (B)

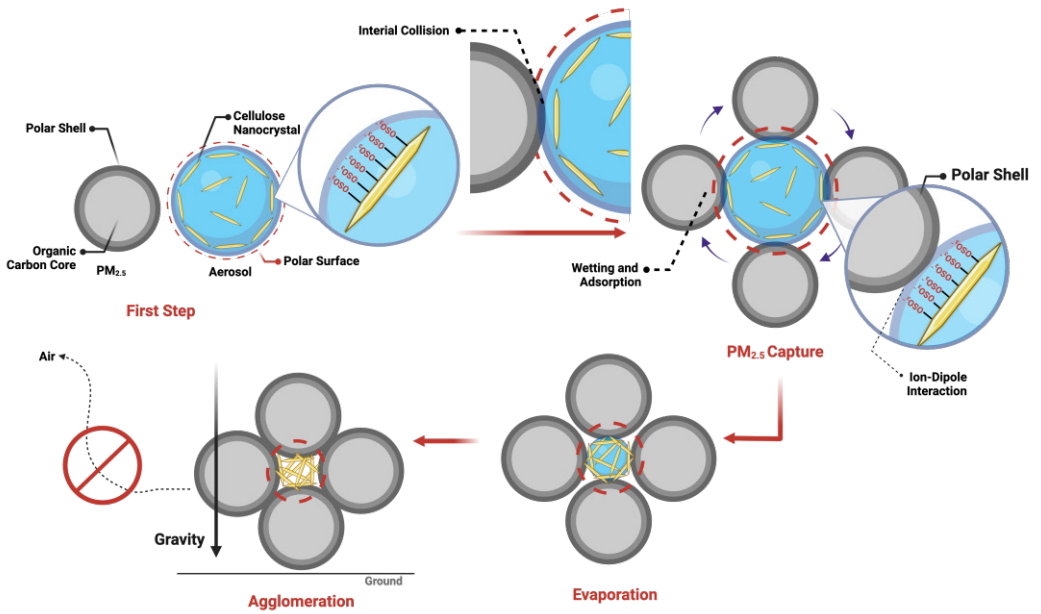

Fig. 7 The proposed $PM_{2.5}$ scavenging mechanism by colloidal BCNC suspension

Conclusion

The potential application of colloidal bacterial cellulose nanocrystal suspensions as a sprayable $PM_{2.5}$ scavenger is demonstrated in this work. Cellulose nanocrystals could be prepared by the sulfuric acid hydrolysis of bacterial cellulose pellicles. Cellulose nanocrystals possessed a needle shape with an average hydrodynamic diameter of 320 nm. The surfaces of cellulose nanocrystals were negatively charged with an average zeta potential of −56.8 mV. The colloidal suspension of negatively charged bacterial cellulose nanocrystals could be aerosolized and applied as a $PM_{2.5}$ capture agent. The aerosolized colloidal bacterial cellulose nanocrystal suspension exhibited considerable interactions with $PM_{2.5}$ and displayed high $PM_{2.5}$ removal efficiency of 78%.

Acknowledgments

This research project was supported and funded by Faculty of Applied Science, King Mongkut's University of Technology North Bangkok, Thailand, contract No. 652092 and Department of Industrial Chemistry, Faculty of Applied Science, King Mongkut's University of Technology North Bangkok, Thailand.

References

Abdelrahman, M.A., Elberry, A.A., Hussein, R.R.S., & Abdelrahim, M.E. (2020). Effect of holding chamber as an add-on device on aerosol delivery and fugitive Aerosol from different jet nebulizers. *Journal of Pharmaceutical Innovation, 15*(1), 73–79.

Apte, J.S., Marshall, J.D., Cohen, A.J., & Brauer, M. (2015). Addressing global mortality from ambient $PM_{2.5}$. *Environmental Science & Technology, 49*(13), 8057–8066.

Arserim-Uçar, D.K., Korel, F., Liu, L., & Yam, K.L. (2021). Characterization of bacterial cellulose nanocrystals: Effect of acid treatments and neutralization. *Food Chemistry, 336,* 127597.

Bałaga, D., Siegmund, M., Kalita, M., Williamson, B.J., Walentek, A., & Małachowski, M. (2021). Selection of operational parameters for a smart spraying system to control airborne PM10 and $PM_{2.5}$ dusts in underground coal mines. *Process Safety and Environmental Protection, 148,* 482–494.

Benini, K.C.C.d.C., Voorwald, H.J.C., Cioffi, M.O.H., Rezende, M.C., & Arantes, V. (2018). Preparation of nanocellulose from Imperata brasiliensis grass using Taguchi method. *Carbohydrate Polymers, 192,* 337-346.

Bhattacharjee, S. (2016). DLS and zeta potential – What they are and what they are not? *Journal of Controlled Release, 235,* 337–351.

Blanco, P.H., Lad, J.B., Bridgwater, A.V., & Holm, M.S. (2018). Production of glucose from the acid hydrolysis of anhydrosugars. *ACS Sustainable Chemistry & Engineering, 6*(10), 12872–12883.

Borowski, G., Smirnov, Y., Ivanov, A., & Danilov, A. (2022). Effectiveness of carboxymethyl cellulose solutions for dust suppression in the mining industry. *International Journal of Coal Preparation and Utilization, 42*(8), 2345-2356.

Bouchard, J., Méthot, M., Fraschini, C., & Beck, S. (2016). Effect of oligosaccharide deposition on the surface of cellulose nanocrystals as a function of acid hydrolysis temperature. *Cellulose, 23*(6), 3555–3567.

Braun, B., & Dorgan, J.R. (2009). Single-step method for the isolation and surface functionalization of cellulosic nanowhiskers. *Biomacromolecules, 10*(2), 334–341.

Cai, J., Yu, W., Li, B., Yao, R., Zhang, T., Guo, M., . . . Kipen, H. (2019). Particle removal efficiency of a household portable air cleaner in real-world residences: A single-blind cross-over field study. *Energy and Buildings, 203,* 109464.

Carotenuto, C., Di Natale, F., & Lancia, A. (2010). Wet electrostatic scrubbers for the abatement of submicronic particulate. *Chemical Engineering Journal, 165*(1), 35–45.

Chang, P., Chen, Y., Xu, G., Huang, J., Ghosh, A., & Liu, W.V. (2021). Numerical study of coal dust behaviors and experimental investigation on coal dust suppression efficiency of surfactant solution by using wind tunnel tests. *Energy Sources, Part A: Recovery, Utilization, and Environmental Effects, 43*(17), 2173–2188.

Delepierre, G., Vanderfleet, O.M., Niinivaara, E., Zakani, B., & Cranston, E.D. (2021). Benchmarking cellulose nanocrystals part II: New industrially produced materials. *Langmuir, 37*(28), 8393–8409.

Endes, C., Mueller, S., Kinnear, C., Vanhecke, D., Foster, E.J., Petri-Fink, A., . . . Rothen-Rutishauser, B. (2015). Fate of cellulose nanocrystal aerosols deposited on the lung cell surface in vitro. *Biomacromolecules, 16*(4), 1267-1275.

Fachri, B.A., Abdilla, R.M., Bovenkamp, H.H.v.d., Rasrendra, C.B., & Heeres, H.J. (2015). Experimental and kinetic modeling studies on the sulfuric acid catalyzed conversion of d-fructose to 5-hydroxymethylfurfural and levulinic acid in water. *ACS Sustainable Chemistry & Engineering, 3*(12), 3024–3034.

Fan, X., Wang, Y., Zhong, W.-H., & Pan, S. (2019). Hierarchically structured all-biomass air filters with high filtration efficiency and low air pressure drop based on pickering emulsion. *ACS Applied Materials & Interfaces, 11*(15), 14266–14274.

Fantke, P., McKone, T.E., Tainio, M., Jolliet, O., Apte, J.S., Stylianou, K.S., . . . Evans, J.S. (2019). Global effect factors for exposure to fine particulate matter. *Environmental Science & Technology, 53*(12), 6855–6868.

Feng, S., Gao, D., Liao, F., Zhou, F., & Wang, X. (2016). The health effects of ambient $PM_{2.5}$ and potential mechanisms. *Ecotoxicology and Environmental Safety, 128,* 67–74.

Gao, J., Woodward, A., Vardoulakis, S., Kovats, S., Wilkinson, P., Li, L., . . . Liu, Q. (2017). Haze, public health and mitigation measures in China: A review of the current evidence for further policy response. *Science of The Total Environment, 578,* 148–157.

Habibi, Y., Chanzy, H., & Vignon, M.R. (2006). TEMPO-mediated surface oxidation of cellulose whiskers. *Cellulose, 13*(6), 679–687.

Habibi, Y., Lucia, L.A., & Rojas, O.J. (2010). Cellulose nanocrystals: Chemistry, self-assembly, and applications. *Chemical Reviews, 110*(6), 3479-3500.

Han, J., Zhou, C., Wu, Y., Liu, F., & Wu, Q. (2013). Self-assembling behavior of cellulose nanoparticles during freeze-drying: Effect of suspension concentration, particle Size, crystal structure, and surface charge. *Biomacromolecules, 14*(5), 1529–1540.

Henrique, M.A., Flauzino Neto, W.P., Silvério, H.A., Martins, D.F., Gurgel, L.V.A., Barud, H.d.S., . . . Pasquini, D. (2015). Kinetic study of the thermal decomposition of cellulose nanocrystals with different polymorphs, cellulose I and II, extracted from different sources and using different types of acids. *Industrial Crops and Products, 76,* 128–140.

Henrique, M.A., Silvério, H.A., Flauzino Neto, W.P., & Pasquini, D. (2013). Valorization of an agro-industrial waste, mango seed, by the extraction and characterization of its cellulose nanocrystals. *Journal of Environmental Management, 121,* 202–209.

Hung, S.-H., Bowden, J.W., Peltier, R.E., & Schiffman, J.D. (2021). Optimizing the packing density and chemistry of cellulose nanofilters for high-efficiency particulate removal. *Industrial & Engineering Chemistry Research, 60*(43), 15720–15729.

Jordan, J.H., Easson, M.W., Dien, B., Thompson, S., & Condon, B.D. (2019). Extraction and characterization of nano-cellulose crystals from cotton gin motes and cotton gin waste. Cellulose, 26(10), 5959–5979.

Kargarzadeh, H., Ahmad, I., Abdullah, I., Dufresne, A., Zainudin, S.Y., & Sheltami, R.M. (2012). Effects of hydrolysis conditions on the morphology, crystallinity, and thermal stability of cellulose nanocrystals extracted from kenaf bast fibers. *Cellulose, 19*(3), 855-866.

Kim, D., & Lee, S.J. (2020). Effect of water microdroplet size on the removal of indoor particulate matter. *Building and Environment, 181,* 107097.

Kim, J., Kim, J.J., & Lee, S.J. (2020). Efficient removal of indoor particulate matter using water microdroplets generated by a MHz-frequency ultrasonic atomizer. *Building and Environment, 175,* 106797.

Klemm, D., Cranston, E.D., Fischer, D., Gama, M., Kedzior, S.A., Kralisch, D., . . . Rauchfuß, F. (2018). Nanocellulose as a natural source for groundbreaking applications in materials science: Today's state. *Materials Today, 21*(7), 720–748.

Kuo, P.-H., Tsuang, B.-J., Chen, C.-J., Hu, S.-W., Chiang, C.-J., Tsai, J.-L., . . . Ku, K.-C. (2014). Risk assessment of mortality for all-cause, ischemic heart disease, cardiopulmonary disease, and lung cancer due to the operation of the world's largest coal-fired power plant. *Atmospheric Environment, 96,* 117-124.

Lee, J.-B., Kim, K.-H., Kim, H.-J., Cho, S.-J., Jung, K., & Kim, S.-D. (2011). Emission rate of particulate matter and its removal efficiency by precipitators in under-fired charbroiling restaurants. *The ScientificWorldJOURNAL, 11,* 1077-1088.

Lee, T., Kim, S., Kim, S., Kwon, N.-Y., Rho, S., Hwang, D.S., . . . Kim, M. (2020). Environmentally friendly methylcellulose-based binders for active and passive dust control. *ACS Applied Materials & Interfaces, 12*(45), 50860–50869.

Li, R., Li, C., Zhuang, J., Zhu, H., Fang, L., & Sun, D. (2020). Mechanistic influence of chemical agglomeration agents on removal of inhalable particles from coal combustion. *ACS Omega, 5*(40), 25906–25912.

Li, S., Zhao, B., Lin, H., Shuang, H., Kong, X., & Yang, E. (2021). Review and prospects of surfactant-enhanced spray dust suppression: Mechanisms and effectiveness. *Process Safety and Environmental Protection, 154,* 410–424.

Liu, C., Hsu, P.-C., Lee, H.-W., Ye, M., Zheng, G., Liu, N., . . . Cui, Y. (2015). Transparent air filter for high-efficiency $PM_{2.5}$ capture. *Nature Communications, 6*(1), 6205.

Mandal, A., & Chakrabarty, D. (2011). Isolation of nanocellulose from waste sugarcane bagasse (SCB) and its characterization. *Carbohydrate Polymers, 86*(3), 1291–1299.

Mata, T.M., Martins, A.A., Calheiros, C.S.C., Villanueva, F., Alonso-Cuevilla, N.P., Gabriel, M.F., . . . Silva, G.V. (2022). Indoor air quality: A review of cleaning technologies. *Environments, 9*(9), 118.

Mintz, D. (2018). *Technical assistance document for the reporting of daily air quality-the air quality index (AQI): US Environmental Protection Agency. Office of Air Quality Planning and Standards, Research Triangle Park, NC: Air Quality Assessment Division. Publication No. EPA-454/B-18-007.*

Mudalige, T., Qu, H., Van Haute, D., Ansar, S.M., Paredes, A., & Ingle, T. (2019). Chapter 11 - Characterization of nanomaterials: Tools and challenges. In A. López Rubio, M. J. Fabra Rovira, M. martínez Sanz, & L. G. Gómez-Mascaraque (Eds.), *Nanomaterials for Food Applications* (pp. 313–353). Elsevier.

Ngoensawat, U., Parnsubsakul, A., Kaitphaiboonwet, S., Wutikhun, T., Sapcharoenkun, C., Pienpinijtham, P., . . . Ekgasit, S. (2021). Luminescent nanohybrid of ZnO quantum dot and cellulose nanocrystal as anti-counterfeiting ink. *Carbohydrate Polymers, 262,* 117864.

Pui, D.Y.H., Chen, S.-C., & Zuo, Z. (2014). $PM_{2.5}$ in China: Measurements, sources, visibility and health effects, and mitigation. *Particuology, 13,* 1–26.

Reid, M.S., Villalobos, M., & Cranston, E.D. (2017). Benchmarking cellulose nanocrystals: From the laboratory to industrial production. *Langmuir, 33*(7), 1583–1598.

Roman, M. (2015). Toxicity of Cellulose Nanocrystals: A Review. *Industrial Biotechnology, 11*(1), 25-33.

Roman, M., & Winter, W.T. (2004). Effect of sulfate groups from sulfuric acid hydrolysis on the thermal degradation behavior of bacterial cellulose. *Biomacromolecules, 5*(5), 1671–1677.

Salari, M., Sowti Khiabani, M., Rezaei Mokarram, R., Ghanbarzadeh, B., & Samadi Kafil, H. (2019). Preparation and characterization of cellulose nanocrystals from bacterial cellulose produced in sugar beet molasses and cheese whey media. *International Journal of Biological Macromolecules, 122,* 280–288.

Schneider, C.A., Rasband, W.S., & Eliceiri, K.W. (2012). NIH Image to ImageJ: 25 years of image analysis. *Nature Methods, 9*(7), 671–675.

Sharma, A., Thakur, M., Bhattacharya, M., Mandal, T., & Goswami, S. (2019). Commercial application of cellulose nano-composites – A review. *Biotechnology Reports, 21,* e00316.

Sheltami, R.M., Abdullah, I., Ahmad, I., Dufresne, A., & Kargarzadeh, H. (2012). Extraction of cellulose nanocrystals from mengkuang leaves (Pandanus tectorius). *Carbohydrate polymers, 88*(2), 772-779.

Song, C., He, J., Wu, L., Jin, T., Chen, X., Li, R., . . . Mao, H. (2017). Health burden attributable to ambient $PM_{2.5}$ in China. *Environmental Pollution, 223,* 575–586.

Souzandeh, H., Scudiero, L., Wang, Y., & Zhong, W.-H. (2017). A disposable multi-functional air filter: Paper towel/protein nanofibers with gradient porous structures for capturing pollutants of broad species and sizes. *ACS Sustainable Chemistry & Engineering, 5*(7), 6209–6217.

Udomsri, C., Sapcharoenkun, C., Ekgasit, S., & Parnklang, T. (2023). Cellulose nanocrystals as renewable materials for suppressing hazardous $PM_{2.5}$ pollution [10.1039/D2NJ05452C]. *New Journal of Chemistry, 47*(7), 3591–3605.

Vasconcelos, N.F., Feitosa, J.P.A., da Gama, F.M.P., Morais, J.P.S., Andrade, F.K., de Souza Filho, M.d.S.M., . . . Rosa, M.d.F. (2017a). Bacterial cellulose nanocrystals produced under different hydrolysis conditions: Properties and morphological features. *Carbohydrate Polymers, 155,* 425–431.

Vasconcelos, N.F., Feitosa, J.P.A., da Gama, F.M.P., Morais, J.P.S., Andrade, F.K., de Souza Filho, M.d.S.M., . . . Rosa, M.d.F. (2017b). Bacterial cellulose nanocrystals produced under different hydrolysis conditions: Properties and morphological features. *Carbohydrate Polymers, 155,* 425-431.

Wang, H., Nie, W., Zhang, H., Jin, H., Bao, Q., Yan, J., . . . Liu, Q. (2020). A synthesis of a dust suppressant using the cellulose extracted from maize straw. *Starch - Stärke, 72*(3-4), 1900187.

Wang, J.-C. (1998). A novel optical microscope laser light scattering system. *Optics Communications, 155*(4), 236-240.

Wang, P., Han, H., Tian, C., Liu, R., & Jiang, Y. (2020). Experimental study on dust reduction via spraying using surfactant solution. *Atmospheric Pollution Research, 11*(6), 32–42.

Wang, P., Tan, X., Zhang, L., Li, Y., & Liu, R. (2019). Influence of particle diameter on the wettability of coal dust and the dust suppression efficiency via spraying. *Process Safety and Environmental Protection, 132,* 189-199.

Wang, Q., Wang, D., Wang, H., Han, F., Zhu, X., Tang, Y., . . . Si, W. (2015). Optimization and implementation of a foam system to suppress dust in coal mine excavation face. *Process Safety and Environmental Protection, 96,* 184-190.

Wang, W., Huang, F., & Li, X. (2022). Development of a portal-crane servo-spraying suppression system to reduce dust production at bulk cargo wharf. *International Journal of System Assurance Engineering and Management, 13*(3), 1151-1161.

Wu, A., Hu, X., Ao, H., Chen, Z., Chu, Z., Jiang, T., . . . Wan, Y. (2022). Rational design of bacterial cellulose-based air filter with antibacterial activity for highly efficient particulate matters removal. *Nano Select, 3*(1), 201–211.

Xing, Y.-F., Xu, Y.-H., Shi, M.-H., & Lian, Y.-X. (2016). The impact of PM2.5 on the human respiratory system. *Journal of Thoracic Disease, 8*(1), E69–E74.

Xiong, Z., Lin, J., Li, X., Bian, F., & Wang, J. (2021). Hierarchically structured nanocellulose-implanted air filters for high-efficiency particulate matter removal. *ACS Applied Materials & Interfaces, 13*(10), 12408–12416.

Xu, C., Wang, D., Wang, H., Ma, L., Zhu, X., Zhu, Y., . . . Liu, F. (2019). Experimental investigation of coal dust wetting ability of anionic surfactants with different structures. *Process Safety and Environmental Protection, 121,* 69–76.

Yan, H., Chen, X., Song, H., Li, J., Feng, Y., Shi, Z., . . . Lin, Q. (2017). Synthesis of bacterial cellulose and bacterial cellulose nanocrystals for their applications in the stabilization of olive oil pickering emulsion. *Food Hydrocolloids, 72,* 127–135.

Yuan, M., Nie, W., Zhou, W., Yan, J., Bao, Q., Guo, C., . . . Guo, L. (2020). Determining the effect of the non-ionic surfactant AEO9 on lignite adsorption and wetting via molecular dynamics (MD) simulation and experiment comparisons. *Fuel, 278,* 118339.

Zhang, H., Nie, W., Yan, J., Bao, Q., Wang, H., Jin, H., . . . Liu, Q. (2020). Preparation and performance study of a novel polymeric spraying dust suppression agent with enhanced wetting and coagulation properties for coal mine. *Powder Technology, 364,* 901-914.

Zhang, Q., Li, Q., Young, T.M., Harper, D.P., & Wang, S. (2019). A novel method for fabricating an electrospun poly (vinyl alcohol)/cellulose nanocrystals composite nanofibrous filter with low air resistance for high-efficiency filtration of particulate matter. *ACS Sustainable Chemistry & Engineering, 7*(9), 8706–8714.

Zhang, R., Liu, C., Zhou, G., Sun, J., Liu, N., Hsu, P.-C., . . . Cui, Y. (2018). Morphology and property investigation of primary particulate matter particles from different sources. *Nano Research, 11*(6), 3182-3192.

Zhou, Q., Xu, G., Chen, Y., Qin, B., Zhao, Z., & Guo, C. (2020). The development of an optimized evaluation system for improving coal dust suppression efficiency using aqueous solution sprays. *Colloids and Surfaces A: Physicochemical and Engineering Aspects, 602,* 125104.